Photostability via Sloped Conical Intersections: A Computational Study of the Pyrene Radical Cation

Andrei M. Tokmachev,[†] Martial Boggio-Pasqua,[‡] Michael J. Bearpark,*[,†] and Michael A. Robb[†]

Department of Chemistry, Imperial College London, London SW7 2AZ, United Kingdom, and Laboratoire de Chimie et Physique Quantiques, UMR 5626, IRSAMC, CNRS et Université Toulouse 3, 118 route de Narbonne, 31062 Toulouse, France

Received: May 19, 2008; Revised Manuscript Received: September 9, 2008

The photophysics of the pyrene radical cation, a polycyclic aromatic hydrocarbon (PAH) and a possible source of diffuse interstellar bands (DIBs), is investigated by means of hybrid molecular mechanics−valence bond (MMVB) force field and multiconfigurational CASSCF and CASPT2 ab initio methods. Potential energy surfaces of the first three electronic states D_0, D_1, and D_2 are calculated. MMVB geometry optimizations are carried out for the first time on a cationic system; the results show good agreement with CASSCF optimized structures, for minima and conical intersections, and errors in the energy gaps are no larger than those found in our previous studies of neutral systems. The presence of two easily accessible sloped D_1/D_2 and D_0/D_1 conical intersections suggests the pyrene radical cation is highly photostable, with ultrafast nonradiative decay back to the initial ground state geometry predicted via a mechanism similar to the one found in the naphthalene radical cation.

Introduction

Diffuse interstellar bands (DIBs), ubiquitous absorption features in the spectra of astronomical objects, have been observed as far back as in the early 20th century.[1] Today, some 300 bands are known in the ultraviolet (UV), visible and infrared (IR) spectral regions. For a long time, the origin of the DIBs was unknown. Although it is still very much debated,[2] the current viewpoint is that polycyclic aromatic hydrocarbons (PAHs) and other large carbon-bearing molecules are responsible for the DIBs.[3] In particular, large neutral PAHs and ionized PAHs were proposed to account for a subset of the DIBs.[4−6] However, assigning these bands remains one of the most challenging problems in astrophysical spectroscopy.

In an interstellar medium, a large fraction of PAHs are expected to be ionized by the strong UV radiation present in this environment. The resulting cations absorb lower energy photons than their neutral counterparts,[7] and their abundance in the interstellar medium is due to their remarkable photostability.[8,9] In particular, the primary decay processes for photoexcited radical cations of PAHs are nonradiative,[10−15] i.e, almost all of the excitation energy is converted into heat that is emitted as IR irradiation in the interstellar medium.[8] Thus, PAH cations are currently regarded as serious potential carriers for some of the DIBs.[4−6,8,16]

Most experimental absorption spectra of PAH cations have been recorded in low-temperature inert gas matrices,[17] because of the difficulty of isolating charged species in the gas phase.[18] Thus, computational studies have proved valuable in understanding these spectra. Various theoretical methods, providing calculated vertical excitation energies in good agreement with experimental spectra, have been used. The semiempirical quantum consistent force field/π-electron plus configuration interaction method (QCFF/PI+CI),[19] time-dependent density functional theory (TD-DFT),[17g,20,21] complete active space self-consistent field (CASSCF) method,[22−25] and multireference perturbation theory (CASPT2)[24,25] were all used to study the electronic absorption spectra of small PAH cations.

However, understanding the photophysical behavior of PAH cations, particularly their high photostability, requires mapping the potential energy surfaces (PESs) involved. This entails optimizing excited-state critical structures and locating PES crossings (conical intersections) that provide ultrafast nonradiative decay channels.[26] In particular, we are concerned about the direct accessibility of these conical intersections via small in-plane bond relaxations, which could account for the excited-state lifetimes and emission properties of such systems. These studies have so far been conducted for the benzene[23] and naphthalene[25] radical cations. For the naphthalene cation, a mechanism involving excited-state relaxation from the D_2 state via two consecutive conical intersections was proposed to account for its photostability. In order to perform similar studies on larger, astrophysically important PAH cations, further approximations need to be used to compute the PESs of these systems, as the CASSCF/CASPT2 approach becomes rapidly intractable.

Molecular mechanics−valence bond (MMVB)[27,28] is a type of hybrid quantum mechanics/molecular mechanics (QM/MM) method involving a parameterized Heisenberg Hamiltonian coupled to a classical MM force field, enabling the description of ground and excited electronic states as well as bond formation/breaking processes. The basis of MMVB in application to conjugated hydrocarbons is to use a classical force field for the σ framework and a quantum description for the valence π electrons. This approach has proved successful in describing the ground and first excited states of systems such as styrene,[29] indacene,[30] pyracylene,[31] and of conjugated radicals.[32] Recently we implemented the MMVB method to describe cationic systems.[33] Promising results were obtained to describe PESs of

* Corresponding author. E-mail: m.bearpark@imperial.ac.uk.
† Imperial College London.
‡ Laboratoire de Chimie et Physique Quantiques, UMR 5626, IRSAMC.

10.1021/jp8044109 CCC: $40.75
Published on Web 10/03/2008

benzene, naphthalene, anthracene, and phenanthrene radical cations based on relaxation pathways obtained at the CASSCF level.[33] However, no explicit geometry optimization was performed using MMVB itself at this time, as the analytical energy gradient had not been implemented for cationic systems, until now. We use MMVB in preference to TD-DFT for these systems at present because, for neutral systems, MMVB can reproduce excited-state geometry changes and crossing geometries reliably,[28] whereas TD-DFT is less reliable at present.[26f]

Because the pyrene radical cation (denoted $Py\bullet^+$) is often considered to be a strong candidate for one of the DIB carriers,[17b,34−36] we propose in this work to use the MMVB method to study the photophysics of this species. We optimize critical points on the ground and first two electronic excited-state PESs of an isolated $Py\bullet^+$ as we have now implemented the MMVB analytical energy gradient for cations. After initial photoexcitation to an absorbing electronic excited state D_n, the system quickly decays back to the first excited state D_1 (consistent with Kasha's rule),[37] where further ultrafast nonradiative decay to the ground state D_0 takes place at an easily accessible sloped conical intersection, D_0/D_1 CI. This mechanism therefore predicts a high photostability for $Py\bullet^+$. Benchmark CASSCF/CASPT2 calculations were also performed in order to assess the accuracy of the MMVB results.

After a discussion of computational methods, we present in detail the results of our MMVB study. A comparison with ab initio CASSCF and CASPT2 results is then described. In conclusion, the experimentally observed photostability[9] of the $Py\bullet^+$ cation is then rationalized, on the basis of our results.

Computational Details

If one seeks a qualitative picture of a photophysical mechanism, or better, a quantitative agreement with the existing experimental data, a thorough analysis of the excited states is of paramount importance. This leads to serious constraints on the nature of the computational tool to be used. Although the one-electron approximation often provides good models for studying simple excitations, it is unreliable, because so many problems involve interaction of many configurations and require essentially multiconfigurational methods. A natural choice of computational tool for analyzing the electronic states and PESs of PAH radical cations would be the CASSCF method, because it fully accounts for configuration interactions within a π-electron system (orbital active space) and provides a reliable description of the rest of the molecule. However, the size of the Hamiltonian matrix produces a major bottleneck in multiconfigurational studies of larger molecules: CASSCF presently has a practical limit of around 10^7 configuration state functions (e.g., $Py\bullet^+$ with 15 electrons in 16 active orbitals and D_{2h} point group symmetry).

A less expensive option can be provided, for example, by density functional computations, but, for a balanced representation of excited state PESs, it is still preferable to rely upon an intrinsically multiconfigurational approach. We use the MMVB[27] method for such systems, which provides reliable results for PESs of a few of the lowest electronic states. This is a hybrid QM/MM method,[28,38,39] where a small part of the system is described by a QM method (in the case of MMVB, this description is based on a valence bond wave function), while the rest is accounted for by classical force fields. In the framework of MMVB, only perfect-pairing covalent electronic configurations are retained, while all of the ionic configurations are omitted explicitly. Of course, such a restriction on the configurations leads to a serious modification of the Hamiltonian, which becomes expressed through VB Coulomb and exchange integrals that can be parameterized from CASSCF calculations. However, the resulting method is much faster than CASSCF for comparable active orbital spaces.[28] This approach has proved to be a unique tool for studying excited-state reactivity in both static and dynamic calculations.[40−43]

Recently we extended the MMVB method to cationic systems,[33] namely, to active spaces with $n - 1$ electrons in n orbitals. In this particular case, each configuration is defined by the position of the hole and the spin factors of $n - 1$ electrons in the other $n - 1$ orbitals. We developed an efficient procedure for generating the Hamiltonian matrices expressed on the basis of many-electron covalent configurations and found a consistent set of parameters for Coulomb, exchange, electron hopping, and three-center integrals arising in the problem. The algorithm is currently implemented in the framework of the development version of the Gaussian program suite.[44] The program allows finding stationary points and conical intersections on PESs by using the analytical gradients of the MMVB energy. In the case of a pyrene radical cation, the number of covalent configurations (Slater determinants) generated from an active space of 15 electrons in 16 orbitals is 102 960, and a single point calculation takes only a few seconds. This time scale greatly contrasts that of the CASSCF method.

The MMVB method for cationic systems has been parameterized for in-plane distortions on the basis of CASSCF calculations for simple two-electron systems.[33] It has been previously applied only to single-point calculations of benzene, naphthalene, anthracene, and phenanthrene radical cations, for some characteristic spatial structures determined through CASSCF calculations, which are possible for these systems.[33] Although the results of MMVB and CASSCF calculations were in good agreement, MMVB was not tested as a predictive tool, as explicit geometry optimizations could not be carried out at that time. Therefore, the full MMVB analysis of the lowest D_0, D_1, and D_2 PESs of $Py\bullet^+$ presented here represents not only a practical application, with the aim to understand the photophysical behavior of the system, but it is also the first real test for this extension of the MMVB method. MMVB geometry optimizations were carried out with constrained planarity due to the lack of reliable parameters for out-of-plane distortions. However, these distortions were not found to be important in the similar relaxation mechanisms of the naphthalene radical cation.[25]

To assess the accuracy of the MMVB results, benchmark CASSCF and CASPT2 calculations were also performed on the D_0, D_1, and D_2 PESs using MOLPRO.[45] The full π active space was chosen at the CASSCF level, i.e., 15 π electrons are distributed in 16 valence π orbitals (15*e*, 16*o*). CASSCF geometry optimizations were performed within the D_{2h} symmetry point group, as all the MMVB structures optimized (with planar constraints) belonged to this point group. Conical intersections were optimized with CASSCF using a reduced (13*e*, 14*o*) active space, as computationally expensive orbital state-averaging procedures are required for such calculations. CASSCF energies with the full (15*e*, 16*o*) active space were then computed at the resulting surface crossing structures. CASPT2 energy calculations were performed at CASSCF optimized geometries to take into account dynamic electron correlation. For such energy computations to be feasible, we also had to reduce the reference space to (13*e*, 14*o*), keeping the CASSCF optimized orbitals frozen with the (15*e*, 16*o*) active space. The basis set used was 6-31G*,[46] which includes polarization *d* functions on the carbon atoms.

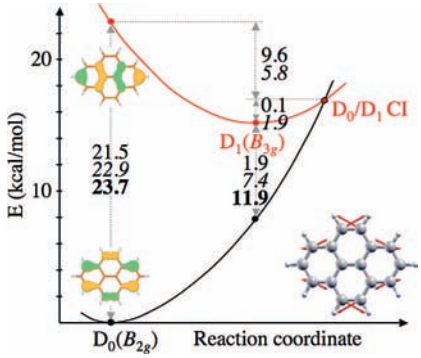

Figure 1. Potential energy profile for the ground (D_0) and first excited (D_1) states of the pyrene radical cation along the D_1 decay pathway. Energy differences are in kcal/mol. Normal, italic, and bold fonts correspond to MMVB, CASSCF (used for energy scale), and CASPT2 values, respectively. "Singly-occupied" molecular orbitals are shown for both electronic states.

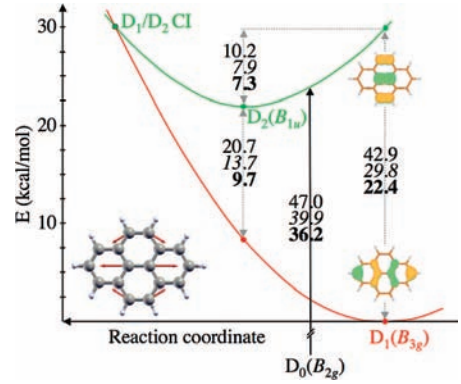

Figure 2. Potential energy profile for the first (D_1) and second excited (D_2) states of the pyrene radical cation along the D_2 decay pathway. Energy differences are in kcal/mol. Normal, italic, and bold fonts correspond to MMVB, CASSCF (used for energy scale), and CASPT2 values, respectively. "Singly-occupied" molecular orbitals are shown for both electronic states. Zero energy set to D_1 minimum.

The CASSCF derivative coupling vector was not computed to optimize conical intersections here, because it was not needed, as symmetry was used and the upper and lower electronic states belong to different irreducible representations of the D_{2h} point group. This substantially reduces the computational cost, but means that we cannot compare CASSCF and MMVB derivative coupling vectors.

Results and Discussion

MMVB Results. In our analysis of the electronic structures of $Py\bullet^+$, we restricted ourselves to the three lowest electronic states and studied the topology of their PESs. We performed a series of MMVB calculations to find the minima for the ground (D_0) and first two excited (D_1 and D_2) states as well as the corresponding conical intersections (D_0/D_1 CI and D_1/D_2 CI). Therefore, we concentrate on the five characteristic spatial structures on the PESs and the relative energies of the states D_0, D_1, and D_2. The absolute MMVB energies at the respective optimized structures are tabulated in Table S1 in the Supporting Information.

The excitation energies are well established on the basis of the corresponding photoelectron spectrum[47] and the electronic absorption spectrum.[48,49] The vertical excitation energies for the transitions $D_0 \rightarrow D_1$ (symmetry-forbidden) and $D_0 \rightarrow D_2$ (symmetry-allowed) are 19.6[47] and 36.7,[47] 36.4,[48] 35.7,[49] kcal/mol, respectively. These quantities were also theoretically analyzed in a series of studies,[19,20a,b] and the computed values are typically somewhat larger than the experimental ones: for example, (25.4, 39.7) and (24.5, 37.4)[20a] using TD-DFT and (27.0, 41.3)[19] using the QCFF/PI method. Figures 1 and 2 show that the corresponding MMVB transitions are 21.5 and 47.0 kcal/mol, respectively. Thus, MMVB describes the first excited state better than the second one. This is not surprising, because our experience based on MMVB calculations of smaller systems is that the MMVB method describes the ground and first excited singlet state PESs well, while the quality of the electronic wavefunction deteriorates for higher excited states.

Although our MMVB calculations were performed with only restriction of planarity on the geometry of the system, all the optimized minima and conical intersections belong to the D_{2h} symmetry point group. The optimized spatial structures can be characterized by the variations of the bond lengths. There are six different bond lengths in D_{2h} $Py\bullet^+$. Table 1 shows these bond lengths for all five optimized geometry configurations, and Figure S1 in the Supporting Information displays these structures. To describe the bonds, we use the numbering system for carbon atoms based on the IUPAC rules for fused rings, as shown in Chart 1. One can see that the minima for the ground and excited states differ noticeably, as discussed in more detail below. The charge distributions determined for each structure (Table S2 in Supporting Information) also illustrate the distinct electronic character of the states. The main observation is that the charge patterns for a particular state do not change significantly when the geometry varies. (The only exception is for the D_2 state, where the charge distribution changes significantly when the geometry approaches the D_1 minimum).

We first discuss the MMVB D_0 and D_1 potential energy profiles, as shown in Figure 1. (The comparison with CASSCF and CASPT2 results is given in the next subsection). The transition from the ground to the first excited state minimum is

TABLE 1: MMVB and CASSCF (in Italics) Bond Lengths[a] (Å) in Pyrene Radical Cation for D_0, D_1, and D_2 PES Minima and D_0/D_1 and D_1/D_2 Conical Intersections

geometry	1−2	3−3a	3a−3a^1	3a−4	4−5	3a^1−5a^1
D_0 minimum	1.399	1.429	1.422	1.420	1.392	1.422
	1.392	*1.422*	*1.419*	*1.415*	*1.383*	*1.416*
D_1 minimum	1.420	1.386	1.448	1.459	1.358	1.381
	1.406	*1.385*	*1.446*	*1.450*	*1.353*	*1.395*
D_2 minimum	1.403	1.417	1.422	1.431	1.410	1.481
	1.394	*1.405*	*1.427*	*1.423*	*1.391*	*1.474*
D_0/D_1 CI	1.422	1.382	1.450	1.463	1.354	1.378
	1.412	*1.369*	*1.458*	*1.466*	*1.339*	*1.372*
D_1/D_2 CI	1.389	1.452	1.402	1.400	1.463	1.546
	1.378	*1.427*	*1.403*	*1.394*	*1.433*	*1.542*

[a] Bond lengths not explicitly defined are equivalent in D_{2h} symmetry.

CHART 1: Partial Atom Numbering for Pyrene, Based on IUPAC Rules

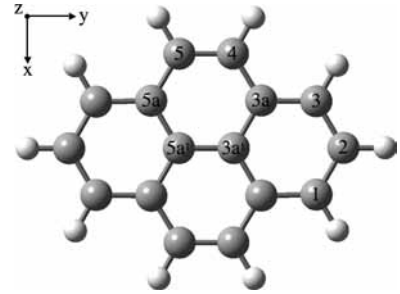

characterized by a significant geometry change, which can be viewed as a contraction of the 3−3a, $3a^1-5a^1$ and 4−5 bonds, with the 4−5 bond clearly acquiring a strong double-bond character (1.36 Å). The remaining 1−2, 3a−$3a^1$, and 3a−4 bonds become elongated. The adiabatic excitation energy is 11.7 kcal/mol, and is significantly smaller than the vertical excitation energy, attesting to the important relaxation energy on the D_1 PES. Remarkably, the D_0-D_1 energy gap at the D_1 minimum is very small (1.9 kcal/mol with MMVB). This is a hint that there is a state crossing along the $D_0 \rightarrow D_1$ reaction path, which we find very close to the D_1 minimum. This D_0/D_1 conical intersection lies only 0.1 kcal/mol above the D_1 minimum, at a very similar geometry, and is therefore predicted to be easily accessible.[40]

This picture can be useful in the understanding of the photorelaxation mechanism from the D_1 state. An important characteristic of conical intersections between PESs is that they can serve as funnels between electronic states, providing ultrafast nonradiative transition channels.[26] The topology of the conical intersection is important for studying the excited state reactivity and photophysics. The calculated D_0/D_1 CI for $Py^{\bullet+}$ is "sloped" (according to the classification system of Ruedenberg),[50] which means that the single relaxation coordinate on D_0 after decay corresponds to the downhill slope on both PESs. Taking the easy access of the CI into account, one can expect ultrafast radiationless relaxation from D_1.

However, it is necessary to mention that the $D_0 \rightarrow D_1$ transition is symmetry-forbidden. Using the orientation of $Py^{\bullet+}$ as shown in Chart 1, D_0 belongs to the B_{2g} irreducible representation, while D_1 belongs to B_{3g}. It has been suggested that photoexcitation of $Py^{\bullet+}$ populates the D_5 state of A_u symmetry[48] (although some TD-DFT spectra[20a,b] do not support this assignment). Relaxation of the first excited state is of course relevant, as it is usually assumed that there is a rapid $D_n \rightarrow D_1$ nonradiative transition[9,37] and the electronic deactivation depends on the $D_1 \rightarrow D_0$ transition. This simple model (for which there are well-documented exceptions; see, for example, ref 40) assumes that the energy gaps between the states D_{n-1} and D_n are relatively small in comparison with the gap between the states D_0 and D_1, and that $D_n \rightarrow D_1$ nonradiative conversion occurs in cascade via dense vibronic levels without necessary involvement of conical intersections. However, in our case, D_2 lies 25.6 kcal/mol above D_1 at the ground-state geometry, and this energy gap remains higher than 20 kcal/mol at the D_2 minimum according to our MMVB calculations (Table S1). Therefore, it would be useful to provide a relaxation mechanism of the D_2 state (see Figure 2) to show that radiationless decay is possible from a state that can be optically excited.

The D_2 state is of B_{1u} symmetry and represents the first excited state whose transition from D_0 is not symmetry-forbidden. However, the corresponding oscillator strength is relatively small compared to the $D_5(2A_u)$ state (20 and 12 times smaller given by electronic absorption spectrum[48] and TD-DFT spectrum,[20a] respectively). The geometry of the D_2 minimum is characterized by an elongated $3a^1-5a^1$ central bond (see Table 1), all the other bond lengths being similar to the ones found for the D_0 minimum. The adiabatic excitation energy is 44.5 kcal/mol, which is only 2.5 kcal/mol less than the vertical excitation energy. This small relaxation energy on D_2 reflects the fact that the D_0 and D_2 minima display similar structures. A direct consequence is that the D_0-D_2 energy gap is reduced by only 4.9 kcal/mol when moving from the D_0 minimum to the D_2 minimum. On the other hand, the D_1-D_2 energy gap is more sensitive to geometry relaxation: at the D_1 minimum it is 42.9 kcal/mol, but it is reduced to 20.7 kcal/mol at the D_2 minimum, as shown in Figure 2. These significant variations suggest that we can find a D_1/D_2 crossing if we change the geometry further along the path from the D_1 minimum to the D_2 minimum, a coordinate that involves mainly the elongation of the $3a^1-5a^1$ and 4−5 bonds. Indeed, the optimized D_1/D_2 CI confirms this hypothesis (see the changes of bond lengths in Table 1, and Figure 2). It is remarkable that the central bond becomes particularly long: 1.546 Å, which is even longer than the equilibrium bond distance for a single C−C bond in the molecular mechanics force field used to describe the σ-core. The most important result is that this D_1/D_2 conical intersection is sloped and it should be readily accessible following initial photoexcitation to the D_5 band,[48] as it is only 7.9 kcal/mol higher in energy than the D_2 minimum.

Benchmark CASSCF and CASPT2 Results. CASSCF and CASPT2 calculations were performed to assess the reliability of the MMVB PESs obtained for the D_0, D_1, and D_2 electronic states. Before we start comparing the results, it should be noted that the MMVB force field is parameterized to reproduce CASSCF calculations and not experimental or CASPT2 results. However, a thorough study of the excited states of the naphthalene radical cation has demonstrated previously that CASSCF calculations cannot be completely adequate, and that inclusion of dynamic electron correlation via CASPT2 may be important to reproduce the experimental excited states.[25]

Table 1 collects the bond lengths obtained from CASSCF geometry optimizations. The main CASSCF and CASPT2 energetic features are displayed in Figures 1 and 2 (absolute CASSCF and CASPT2 energies are gathered in Tables S3 and S4). Compared to the CASSCF structures, MMVB provides a very satisfying description of all of the minima and conical intersections. Root-mean-square deviations of 0.006 Å, 0.009 Å, and 0.011 Å are obtained for the six distinct bond lengths of the D_0, D_1, and D_2 minimum geometries shown in Table 1, respectively. Maximum errors are under 0.01 Å for D_0, 0.015 Å for D_1, and 0.02 Å for D_2. The root-mean-square deviation is 0.010 Å for the D_0/D_1 CI with a maximum error of 0.015 Å, comparable to the three minima. However, this increases to 0.017 Å for the D_1/D_2 CI with a maximum error of 0.030 Å, a direct consequence of the poorer MMVB description of energetics of the D_2 state, as we explain below.

Conical intersection geometries are sensitive to the energy difference between the two electronic states involved. CASSCF and CASPT2 vertical excitation energies are 22.9 and 23.7 kcal/mol for the D_1 state, respectively. The MMVB value of 21.5 kcal/mol is in good agreement with these. However, one can see in Figure 1 that the D_0-D_1 energy gap reduces too quickly along the D_1 relaxation pathway with MMVB. At the D_1 minimum, the D_0-D_1 energy gap is only 1.9 kcal/mol with MMVB, against 7.4 and 11.9 kcal/mol with CASSCF and CASPT2, respectively. Consequently, the D_0/D_1 CI lies too close to the D_1 minimum at the MMVB level: only 0.1 kcal/mol above it, against 1.9 kcal/mol with CASSCF.

On the other hand, CASSCF and CASPT2 vertical excitation energies to the D_2 state are 39.9 and 36.2 kcal/mol, respectively, but the MMVB value of 47.0 kcal/mol is clearly too high, the experimental value being ca. 36 kcal/mol. Thus, the D_1-D_2 energy gap is overestimated at the MMVB level, which is at the origin of the larger discrepancy in the D_1/D_2 CI geometry. This can also be seen in Figure 2, where the D_1-D_2 energy gap is too large along the reaction path leading to the surface crossing. Despite this deficiency, the energy difference of the

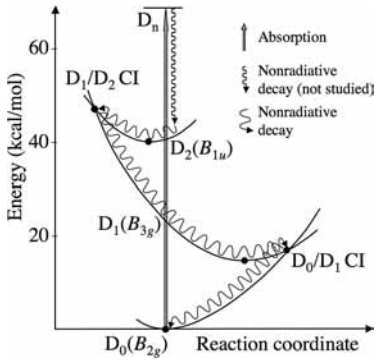

Figure 3. Relaxation mechanism of the pyrene radical cation via two successive "sloped" conical intersections D_1/D_2 CI and D_0/D_1 CI.

D_1/D_2 CI relative to the D_2 minimum is reproduced: 8.1 and 7.9 kcal/mol at the CASSCF and MMVB levels, respectively.

It is worth noting that, at the CASSCF D_0/D_1 CI and D_1/D_2 CI optimized geometries, the two respective electronic states split by over 6 kcal/mol at the CASPT2 level, indicating that differential dynamic electron correlation is not negligible. This effect was already observed in the study of the naphthalene cation.[25] We therefore do not know the real crossing energy and geometry at the CASPT2 level. On the basis of interpolations carried out on the smaller naphthalene cation, we do not expect CASPT2 to increase the energy difference between the minimum and the crossing, although we cannot confirm this by explicit geometry optimization at present.

In addition, MMVB satisfactorily reproduces the topology of the two conical intersections: both are sloped (parallel gradients on upper and lower states) with equivalent gradient difference vectors compared to CASSCF.

Conclusion and Outlook

The photophysics of the pyrene radical cation was studied using the MMVB hybrid force field. PESs of the first three electronic states were investigated. Geometry optimizations of critical points, including conical intersections between the relevant electronic states, were performed using the MMVB analytical energy gradient for the first time in cationic systems. CASSCF geometry optimizations and CASPT2 energy calculations were also performed in order to assess the reliability of the MMVB results: good agreement between MMVB and CASSCF energies and optimized structures, including those of conical intersections, was achieved. In addition, the sloped topology of the conical intersections (parallel gradients and direction of the gradient difference vector) was adequately described. Some energetic features were not accurately reproduced with MMVB, particularly for the D_2 electronic state, which was found to be too high in energy with respect to the D_0 and D_1 electronic states. This discrepancy for higher excited states was already observed in previous studies (see, for example, ref 31) and is due to the less reliable parameterization of MMVB for these states.

Figure 3 summarizes the main relaxation pathways back to the ground state in $Py^{\bullet+}$. Assuming initial photoexcitation to a D_n electronic state (possibly the D_5 band)[48] and rapid deactivation to the lower D_2 state, further rapid deactivation back to D_0 can be accounted for by the presence of two accessible "sloped" conical intersections–D_0/D_1 and D_1/D_2–along the reaction path. (Note that the reaction coordinate in Figure 3 involves distinct in-plane relaxation pathways directed towards crossings, requiring different geometry changes, as shown in Figures 1 and 2). This mechanism provides a rational explanation for the photostability of $Py^{\bullet+}$. A similar mechanism was proposed to account for the photostability of the naphthalene radical cation.[25] However, the two sloped conical intersections involved are even more accessible in $Py^{\bullet+}$, suggesting a shorter excited-state lifetime in this case. Thus, our model also predicts $Py^{\bullet+}$ to be nonfluorescent. We hope therefore that our study will encourage experimental work on the time-resolved photodynamics and emission of the pyrene cation, particularly in the gas phase. We plan to use the MMVB method we have further tested here to study cations of larger PAHs, for which CASSCF calculations are not possible at present.

Acknowledgment. A.M.T. acknowledges the financial support from a Marie Curie Fellowship (Contract No. MIF1-CT-2005-021198). We thank the EPSRC National Service for Computational Chemistry Software (www.nsccs.ac.uk) for providing us with the computing and software resources to perform all of the MOLPRO calculations. We also thank Kate Hall for her comments on this paper.

Supporting Information Available: Cartesian coordinates of all optimized MMVB and CASSCF structures. Tables S1 and S2 show the MMVB energies and charge distributions characterizing the different electronic states, respectively. Tables S3 and S4 are collections of the CASSCF and CASPT2 energies, respectively. Figure S1 shows structures of the optimized critical points with MMVB and CASSCF. This material is available free of charge via the Internet at http://pubs.acs.org.

References and Notes

(1) Heger, M. L. *Lick Obs. Bull.* **1922**, *10*, 146.
(2) Sarre, P. J. *J. Mol. Spectrosc.* **2006**, *238*, 1.
(3) Duley, W. W. *Faraday Discuss.* **2006**, *133*, 415.
(4) Léger, A.; d'Hendecourt, L. *Astron. Astrophys.* **1985**, *146*, 81.
(5) van der Zwet, G. P.; Allamandola, L. *Astron. Astrophys.* **1985**, *146*, 76.
(6) (a) Crawford, M. K.; Tielens, A. G. G. M.; Allamandola, L. J. *Astrophys. J.* **1985**, *293*, L45. (b) Allamandola, L. J.; Tielens, A. G. G. M.; Barker, J. R. *Astrophys. J.* **1985**, *290*, L25.
(7) Shida, T.; Iwata, S. *J. Am. Chem. Soc.* **1973**, *95*, 3473.
(8) Snow, T. P. *Spectochim. Acta, Part A* **2001**, *57*, 615, and references therein.
(9) Zhao, L.; Lian, R.; Shkrob, I. A.; Crowell, R. A.; Pommeret, S.; Chronister, E. L.; Liu, A. D.; Trifunac, A. D. *J. Phys. Chem. A* **2004**, *108*, 25.
(10) (a) Gotkis, Y.; Oleinikova, M.; Naor, M.; Lifshitz, C. *J. Phys. Chem.* **1993**, *97*, 12282. (b) Ho, Y.-P.; Dunbar, R. C.; Lifshitz, C. *J. Am. Chem. Soc.* **1995**, *117*, 6504. (c) Ling, Y.; Lifshitz, C. *J. Mass Spectrosc.* **1997**, *32*, 1219. (d) Jochims, H. W.; Baumgärtel, H.; Leach, S. *Astrophys. J.* **1999**, *512*, 500.
(11) (a) Haselbach, E.; Bally, T. *Pure Appl. Chem.* **1984**, *56*, 1203. (b) Miller, T. *Annu. Rev. Phys. Chem.* **1982**, *33*, 257.
(12) Gumy, J.-C.; Vauthey, E. *J. Phys. Chem. A* **1997**, *101*, 8575.
(13) Brodard, P.; Sarbach, A.; Gumy, J.-C.; Bally, T.; Vauthey, E. *J. Phys. Chem. A* **2001**, *105*, 6594.
(14) Ermolaev, V. L. *Russ. Chem. Rev.* **2001**, *70*, 471.
(15) Medvedev, E. S.; Osherov, V. I. *Radiationless Transitions in Polyatomic Molecules*; Springer-Verlag: New York, 1995.
(16) Salama, F.; Galazutdinov, G. A.; Krelowski, J.; Allamandola, L. J.; Musaev, F. A. *Astrophys. J.* **1999**, *526*, 265.
(17) (a) Salama, F.; Allamandola, L. J. *J. Chem. Phys.* **1991**, *94*, 6964. (b) Salama, F.; Allamandola, L. J. *Astrophys. J.* **1992**, *395*, 301. (c) Salama, F.; Allamandola, L. J. *Nature* **1992**, *358*, 42. (d) Salama, F.; Joblin, C.; Allamandola, L. J. *J. Chem. Phys.* **1994**, *101*, 10252. (e) Ruiterkamp, R.; Halasinski, T.; Salama, F.; Foing, B. H.; Allamandola, L. J.; Schmidt, W.; Ehrenfreund, P. *Astron. Astrophys.* **2002**, *390*, 1153. (f) Chillier, X. D. F.; Stone, B. M.; Joblin, C.; Salama, F.; Allamandola, L. J. *J. Chem. Phys.* **2002**, *116*, 5725. (g) Halasinski, T. M.; Weisman, J. L.; Ruiterkamp, R.; Lee, T. J.; Salama, F.; Head-Gordon, M. *J. Phys. Chem. A* **2003**, *107*, 3660. (h) Rouillé, G.; Arold, M.; Staicu, A.; Krasnokutski, S.; Huisken, F.; Henning, T.; Tan, X.; Salama, F. *J. Chem. Phys.* **2007**, *126*, 174311.

(18) (a) Biennier, L.; Salama, F.; Allamandola, L. J.; Scherer, J. J. *J. Chem. Phys.* **2003**, *118*, 7863. (b) Romanini, D.; Biennier, L.; Salama, F.; Kachanov, A.; Allamandola, L. J.; Stoeckel, F. *Chem. Phys. Lett.* **1999**, *303*, 165.

(19) Negri, F.; Zgierski, M. Z. *J. Chem. Phys.* **1994**, *100*, 1387.

(20) (a) Hirata, S.; Lee, T. J.; Head-Gordon, M. *J. Chem. Phys.* **1999**, *111*, 8904. (b) Hirata, S.; Head-Gordon, M.; Szczepanski, J.; Vala, M. *J. Phys. Chem. A* **2003**, *107*, 4940. (c) Weisman, J. L.; Lee, T. J.; Salama, F.; Head-Gordon, M. *Astrophys. J.* **2003**, *587*, 256. (d) Weisman, J. L.; Mattioda, A.; Lee, T. J.; Hudgins, D. M.; Allamandola, L. J.; Bauschlicher, C. W.; Head-Gordon, M. *Phys. Chem. Chem. Phys.* **2005**, *7*, 109.

(21) (a) Malloci, G.; Mulas, G.; Joblin, C. *Astron. Astrophys.* **2004**, *426*, 105. (b) Malloci, G.; Mulas, G.; Cappellini, G.; Joblin, C. *Chem. Phys.* **2007**, *340*, 43.

(22) Andruniow, T.; Pawlikowski, M. *Chem. Phys.* **1998**, *236*, 25.

(23) Applegate, B. E.; Miller, T. A. *J. Chem. Phys.* **2002**, *117*, 10654.

(24) Bally, T.; Carra, C.; Fülscher, M. P.; Zhu, Z. *J. Chem. Soc., Perkin Trans. 2* **1998**, 1759.

(25) Hall, K. F.; Boggio-Pasqua, M.; Bearpark, M. J.; Robb, M. A. *J. Phys. Chem. A* **2006**, *110*, 13591.

(26) (a) Klessinger, M.; Michl, J. *Excited States and Photochemistry of Organic Molecules*; VCH: New York, 1995; pp 182−186. (b) Blancafort, L.; Ogliaro, F.; Olivucci, M.; Robb, M. A.; Bearpark, M. J.; Sinicropi, A. Computational investigation of photochemical reaction mechanisms. In *Computational Methods in Photochemistry*; Kutateladze, A. G. , Ed.; CRC Press: Boca Raton, FL, 2005. (c) Robb, M. A.; Garavelli, M.; Olivucci, M.; Bernardi, F. A computational strategy for organic photochemistry. In *Reviews in Computational Chemistry*; Lipkowitz, K. B., Boyd, D. B. , Eds.; Wiley-VCH, Inc.: New York, 2000. (d) Bernardi, F.; Olivucci, M.; Robb, M. A. *Chem. Soc. Rev.* **1996**, *25*, 321. (e) Yarkony, D. R. *Rev. Mod. Phys.* **1996**, *68*, 985. (f) Levine, B. G.; Ko, C.; Quenneville, J.; Martinez, T. J. *Mol. Phys.* **2006**, *104*, 1039.

(27) Bernardi, F.; Olivucci, M.; Robb, M. A. *J. Am. Chem. Soc.* **1992**, *114*, 1606.

(28) Bearpark, M. J.; Ogliaro, F.; Vreven, T.; Boggio-Pasqua, M.; Frisch, M. J.; Larkin, S. M.; Morrison, M.; Robb, M. A. *J. Photochem. Photobiol. A* **2007**, *190*, 207.

(29) Bearpark, M. J.; Bernardi, F.; Olivucci, M.; Robb, M. A. *J. Phys. Chem. A* **1997**, *101*, 8395.

(30) Bearpark, M. J.; Celani, P.; Jolibois, F.; Olivucci, M.; Robb, M. A.; Bernardi, F. *Mol. Phys.* **1999**, *96*, 645.

(31) Boggio-Pasqua, M.; Robb, M. A.; Bearpark, M. J. *J. Phys. Chem. A* **2005**, *109*, 8849.

(32) Bearpark, M. J.; Boggio-Pasqua, M. *Theor. Chem. Acc.* **2003**, *110*, 105.

(33) Hall, K. F.; Tokmachev, A. M.; Bearpark, M. J.; Boggio-Pasqua, M.; Robb, M. A. *J. Chem. Phys.* **2007**, *127*, 134111.

(34) Parisel, O.; Berthier, G.; Ellinger, Y. *Astron. Astrophys.* **1992**, *266*, L1.

(35) Szczepanski, J.; Vala, M. *Nature* **1993**, *363*, 699.

(36) Salama, F.; Allamandola, L. J. *J. Chem. Soc., Faraday Trans.* **1993**, *89*, 2277.

(37) Kasha, M. *Discuss. Faraday Soc.* **1950**, *9*, 14.

(38) Sherwood, P. In *Modern Methods and Algorithms of Quantum Chemistry*; John von Neumann Institute for Computing: Jülich, Germany, 2000; pp 285−305.

(39) Tchougréeff, A. L.; Tokmachev, A. M. In *Advanced Topics in Theoretical Chemical Physics*; Kluwer: Dordrecht, 2003, 207−245.

(40) Bearpark, M. J.; Bernardi, F.; Clifford, S.; Olivucci, M.; Robb, M. A.; Smith, B. R.; Vreven, T. *J. Am. Chem. Soc.* **1996**, *118*, 169.

(41) Jolibois, F.; Bearpark, M. J.; Klein, S.; Olivucci, M.; Robb, M. A. *J. Am. Chem. Soc.* **2000**, *122*, 5801.

(42) Boggio-Pasqua, M.; Ravaglia, M.; Bearpark, M. J.; Robb, M. A. *J. Phys. Chem. A* **2003**, *107*, 11139.

(43) Garavelli, M.; Ruggeri, F.; Ogliaro, F.; Bearpark, M. J.; Bernardi, F.; Olivucci, M.; Robb, M. A. *J. Comp. Chem.* **2003**, *24*, 357.

(44) Frisch, M. J.; Trucks, G. W.; Schlegel, H. B.; Scuseria, G. E.; Robb, M. A.; Cheeseman, J. R.; Montgomery, J. A., Jr.; Vreven, T.; Scalmani, G.; Mennucci, B.; Barone, V.; Petersson, G. A.; Caricato, M.; Nakatsuji, H.; Hada, M.; Ehara, M.; Toyota, K.; Fukuda, R.; Hasegawa, J.; Ishida, M.; Nakajima, T.; Honda, Y.; Kitao, O.; Nakai, H.; Li, X.; Hratchian, H. P.; Peralta, J. E.; Izmaylov, A. F.; Kudin.,K. N.; Heyd, J. J.; Brothers, E.; Staroverov, V. N.; Zheng, G.; Kobayashi, R.; Normand, J.; Sonnenberg, J. L.; Ogliaro, F.; Bearpark, M.; Parandekar, P. V.; Ferguson, G. A.; Mayhall, N. J.; Iyengar, S. S.; Tomasi, J.; Cossi, M.; Rega, N.; Burant, J. C.; Millam, J. M.; Klene, M.; Knox, J. E.; Cross, J. B.; Bakken, V.; Adamo, C.; Jaramillo, J.; Gomperts, R.; Stratmann, R. E.; Yazyev, O.; Austin, A. J.; Cammi, R.; Pomelli, C.; Ochterski, J. W.; Ayala, P. Y.; Morokuma, K.; Voth, G. A.; Salvador, P.; Dannenberg, J. J.; Zakrzewski, V. G.; Dapprich, S.; Daniels, A. D.; Strain, M. C.; Farkas, O.; Malick, D. K.; Rabuck, A. D.; Raghavachari, K.; Foresman, J. B.; Ortiz, J. V.; Cui, Q.; Baboul, A. G.; Clifford, S.; Cioslowski, J.; Stefanov, B. B.; Liu, G.; Liashenko, A.; Piskorz, P.; Komaromi, I.; Martin, R. L.; Fox, D. J.; Keith, T.; Al-Laham, M. A.; Peng, C. Y.; Nanayakkara, A.; Challacombe, M.; Chen, W.; Wong, M. W.; Pople, J. A. *Gaussian Development Version*, Revision G.01; Gaussian, Inc.: Wallingford, CT, 2007.

(45) Werner, H.-J.; Knowles, P. J.; Lindh, R.; Schütz, M.; Celani, P.; Korona, T.; Manby, F. R.; Rauhut, G.; Amos, R. D.; Bernhardsson, A.; Berning, A.; Cooper, D. L.; Deegan, M. J. O.; Dobbyn, A. J.; Eckert, F.; Hampel, C.; Hetzer, G.; Lloyd, A. W.; McNicholas, S. J.; Meyer, W.; Mura, M. E.; Nicklass, A.; Palmieri, P.; Pitzer, R.; Schumann, U.; Stoll, H.; Stone, A. J.; Tarroni, R.; Thorsteinsson, T. *MOLPRO*, version 2002.6; University of Birmingham: Birmingham, U.K., 2003.

(46) (a) Hehre, W. J.; Ditchfield, R.; Pople, J. A. *J. Chem. Phys.* **1972**, *56*, 2257. (b) Hariharan, P. C.; Pople, J. A. *Theor. Chim. Acta* **1973**, *28*, 213.

(47) Boschi, R.; Schmidt, W. *Tetrahedron Lett.* **1972**, *25*, 2577.

(48) Vala, M.; Szczepanski, J.; Pauzat, F.; Parisel, O.; Talbi, D.; Ellinger, Y. *J. Phys. Chem.* **1994**, *98*, 9187.

(49) Khan, Z. H. *Spectrochim. Acta, Part A* **1989**, *45*, 253.

(50) Atchity, G. J.; Xantheas, S. S.; Ruedenberg, K. *J. Chem. Phys.* **1991**, *95*, 1862.

JP8044109